A&A 398, 223–228 (2003)
DOI: 10.1051/0004-6361:20021709

Astronomy & Astrophysics

Correlated X–ray timing and spectral behavior in GX 349+2⋆

V. K. Agrawal[1] and S. Bhattacharyya[2,3,⋆⋆]

[1] ISRO Satellite Centre, Airport Road, Bangalore 560 017, India
[2] Joint Astronomy Program, Indian Institute of Science, Bangalore 560012, India
[3] Indian Institute of Astrophysics, Bangalore 560 034, India
e-mail: vivek_isac@yahoo.com; sudip@physics.iisc.ernet.in

Received 27 December 2001 / Accepted 4 November 2002

Abstract. We present a detailed and systematic investigation of correlated spectral and timing properties of the Z source GX 349+2, using extensive data (~221 ks) obtained from the Proportional-Counter-Array on-board RXTE satellite, during January 1998 and September–October 1998. For the first time a detailed comparison between the normal-branch-properties and the flaring-branch-properties of GX 349+2 has been possible, since this study showed the presence of a rare, extended normal branch. Peaked noise properties have been analyzed as functions of position along the Z-track and have been compared to those of Cyg X-2.

Key words. accretion, accretion disks – stars: binaries: close – stars: individual: GX 349+2 – stars: neutron – X–rays: stars

1. Introduction

The bright low-mass X–ray binary (LMXB) GX 349+2 (also called Sco X-2) belongs to a class called Z sources (Hasinger & van der Klis 1989). These are the most luminous X–ray binaries, which are believed to contain neutron stars as accreting objects, since two of them, Cyg X-2 (Smale 1998) and GX 17+2 (Kuulkers et al. 2002), have exhibited type I X–ray bursts characteristic of neutron stars. A Z source traces out a Z-shaped track on a X–ray color-color diagram (CD) and hardness-intensity diagram (HID). The Z-track generally consists of three parts, horizontal branch (HB), normal branch (NB) and flaring branch (FB). It is generally believed that the inferred mass accretion rate increases along the Z-track from HB to FB (Hasinger et al. 1990). So far six Z sources have been discovered, which are further divided into two subclasses: (1) Cyg-like: Cyg X-2, GX 5-1 & GX 340+0, and (2) Sco-like: Sco X-1, GX 349+2 & GX 17+2 (Kuulkers et al. 1994, 1997). Sco-like objects have smaller and slanted HBs (if it exists) and larger FBs, while HBs for Cyg-like sources are comparatively larger and horizontal, and their FBs are generally much smaller. The long term variations in shape and position of Z-track (secular motion) have been observed for Cyg-like sources (Kuulkers et al. 1994, 1996; Kuulkers & van der Klis 1996). It has been suggested that Cyg-like sources are being viewed at higher inclination angle compared to Sco-like sources (Kuulkers et al. 1994) and contain neutron stars of higher magnetic field strength (Psaltis et al. 1995). Quasi-periodic-oscillations (QPOs) and noise components are found in the power spectra of Z sources. These features are generally well-correlated with the position of the source on the Z-track (Hasinger & van der Klis 1989; van der Klis 1995). There are three types of common noise: very-low-frequency-noise (VLFN), low-frequency-noise (LFN) and high-frequency-noise (HFN). QPOs with frequencies in the range 15–60 Hz are generally observed in the HB and in the upper parts of NB (van der Klis 1995). These are called horizontal-branch-oscillations (HBO). A QPO with the frequency in the range 5–8 Hz is observed from the middle part of NB to the NB/FB vertex and is called normal-branch-oscillation (NBO). A sudden increase in centroid frequency (ν_c) of NBO is observed at the NB/FB vertex and according to the common belief, NBO transforms to FBO (flaring-branch-oscillation) at this point (Dieters & van der Klis 2000). As the source moves up along FB, both centroid frequency and full-width-half-maximum (*FWHM*) of FBO increases. In addition to the low-frequency QPOs, kHz QPOs (200–1200 Hz) are also observed for all the Z sources (see van der Klis 2000, for a review).

GX 349+2 is very similar to Sco X-1 in many respects. For example, both objects exhibit strong flaring behavior and the orbital periods are also similar ($P_{\rm orb}$ ~ 18.9 hr for Sco X-1 and ~22 hr for GX 349+2). However, some properties of GX 349+2 are different from those observed for the other five Z sources. First, it has never exhibited a horizontal branch, as seen from current and past observational data. Besides, instead of NBO and FBO (together called N/FBO), a broad peaked noise with a centroid frequency and *FWHM* of around 6 Hz and 10 Hz respectively were observed in its FB (EXOSAT observation; Ponman et al. 1988). It was found that the width of the peaked noise component decreases with increasing

Send offprint requests to: V. K. Agrawal,
e-mail: vivek_isac@yahoo.com

⋆ Tables 1 and 2 are only available in electronic form at http://www.edpsciences.org

⋆⋆ *Present address:* Department of Astronomy, University of Maryland, College Park, MD 20742-2421, USA

intensity. Ponman et al. (1988) also noticed that the strength of the peaked noise is maximum in the intermediate intensity band, i.e., at the NB/FB vertex. However in their work, the lower part of FB and NB could not be differentiated clearly, since they divided the data according to the intensity and not according to the position along the Z-curve. They also investigated the energy dependence of peaked noise properties and found that the rms-strength of peaked noise was higher in the higher energy bands and there was no time lag between hard and soft photons. Observations with GINGA Large-Area-Counter indicate that the width and the centroid frequency of peaked noise component does not vary significantly as the source moves along FB (O'Neill et al. 2001). They found that the strength of the peaked noise is maximum in the lower part of FB (∼10% of the way up the FB) and it becomes weaker as the source moves up the FB. Kuulkers & van der Klis (1998) reported the detection of a similar peaked noise component at the lower part of FB using ∼4 hrs of RXTE observation. A broader and somewhat weaker peaked noise was detected when the source was in NB. They also showed that rms-strength of peaked noise increases with increasing photon energy. Until now, no narrow N/FBO has been detected for GX 349+2.

In spite of being unique (Kuulkers & van der Klis 1998) among the Z sources, GX 349+2 is poorly observed and the least-understood. In this paper, we present the first detailed quantitative study of this source with good quality RXTE-PCA data. In Sect. 2, we describe the observations and analysis procedures. We summarize the results in Sect. 3 and discuss the implications in Sect. 4.

2. Observations and analysis

We analyze RXTE-PCA public archival data obtained during January 1998 and September–October 1998. Details of the observations are given in Table 1. We use the data for which all 5 PCUs were on. The total amount of good data available for our analysis is ∼221 ks. For the data reduction and analysis, we use standard FTOOLS package version 5.0 distributed and maintained by NASA/HEASARC. The standard-2 mode data with time resolution of 16 s and effective energy range of 2–60 keV are used for the spectral analysis. The background subtraction is applied to the data before creating the spectra. The sky_VLE model of epoch 3 for bright source is used to calculate the PCA background. X–ray color-color diagram (CD) and hardness-intensity diagram (HID) are constructed using 256 s averages. The soft color is defined as the ratio of count rates in 3.5–6.4 keV and 2.0–3.5 keV energy bands and hard color is defined as that in 9.7–16.0 keV and 6.4–9.7 keV energy bands. The intensity is defined as the count rate in the 2–16 keV energy band. To define the position of the source along the Z-track, we use the "rank number" or "S_z" parameterization technique, first introduced by Hasinger et al. (1990) with further modifications by others (Hertz et al. 1992; Kuulkers et al. 1994; Dieters & van der Klis 2000). We select the normal points in the CD in such a way that they form a smooth curve. The color-color points in the CD are projected onto this curve. The S_z-parameter for each projected point was calculated by measuring their distance from NB/FB vertex. We choose two reference points: NB/FB vertex (S_z = 2) and the end point of the FB (S_z = 3). The rest of the Z-track is normalized using the length of FB. For the power spectral analysis, we use the data collected in three single bit modes (2.0–5.1, 5.1–6.5, 6.5–8.7 keV) and one event mode (8.7–60 keV) during January 1998 and that collected in one single bit mode (2.0–5.1 keV) and one event mode (5.1–60 keV) during September–October 1998. The power spectra for all observations are created in the energy range 5.1–60 keV since peaked noise feature is more significant in this energy band. The expected white-noise-level (deadtime effect is not taken into account) is subtracted from each power spectrum. Afterwards, the white-noise-level subtracted power spectra are normalized to fractional-rms-squared per Hz. We create power spectra for 8 s intervals and then average over the time intervals (we do not average over disconnected time intervals) that correspond to the change in the mean S_z-parameter by ≤10%. The average power spectra are rebinned afterwards. The power spectra are fitted by a simple power law (representing the VLFN) and a Lorentzian (denoting the peaked noise). To study the energy dependence of noise components, we create power spectra in the energy bands, 2.0–5.1, 5.1–7.0, 7.0–10.0, 10.0–16.0 keV. Errors on the fitting parameters are calculated by using $\Delta\chi^2 = 1.0$ (68% confidence).

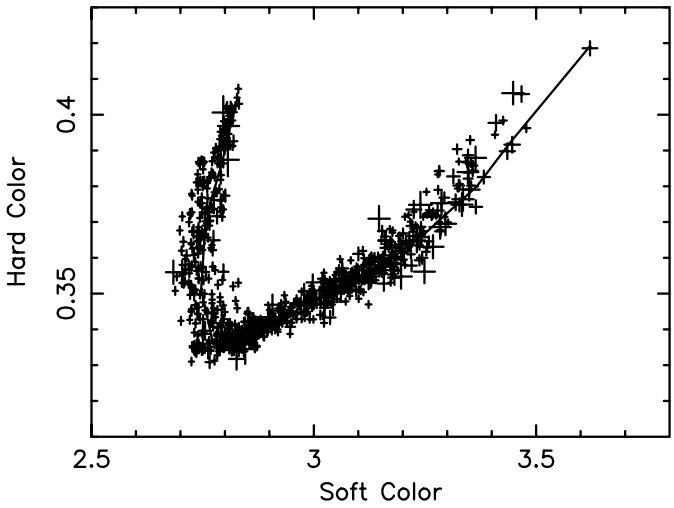

Fig. 1. Combined color-color diagram for observations during January 1998 and September–October 1998. Soft color is the ratio of count rates in the energy band 3.5–6.4 keV and 2–3.5 keV and hard color is that in the energy bands 9.7–16 keV and 6.4–9.7 keV. Each point corresponds to a 256 s bin-size. The solid curve represents an approximate Z-track passing through the normal points.

3. Results

The most complete X–ray color-color diagram of the source GX 349+2 has been obtained from analysis of 31 days of RXTE data. It shows a rare exhibition of an extended NB in this source (Fig. 1). The solid curve in Fig. 1 represents an approximate Z-track passing through the normal points. The hardness-intensity diagram (Fig. 2) shows the intensity of the source increases by a factor of ∼2.5 as it moves from NB/FB vertex to the top of FB. The source occupies different parts and covers

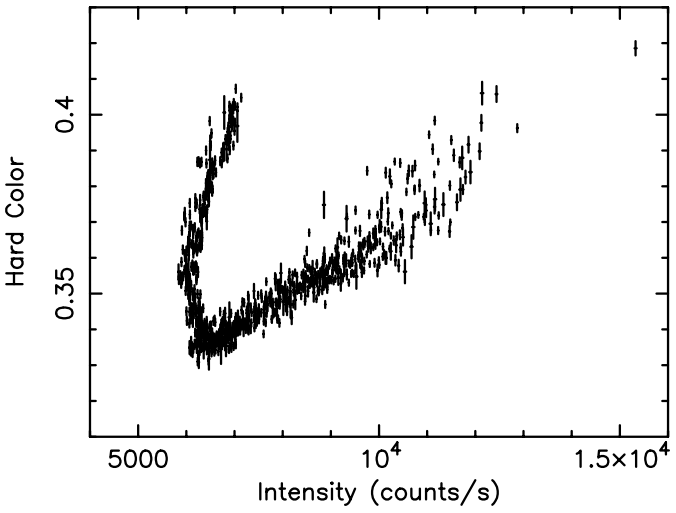

Fig. 2. Combined hardness-intensity diagram for observations mentioned in Fig. 1. The intensity is the count rate in the energy band 2–16 keV. The hard color is same as in Fig. 1.

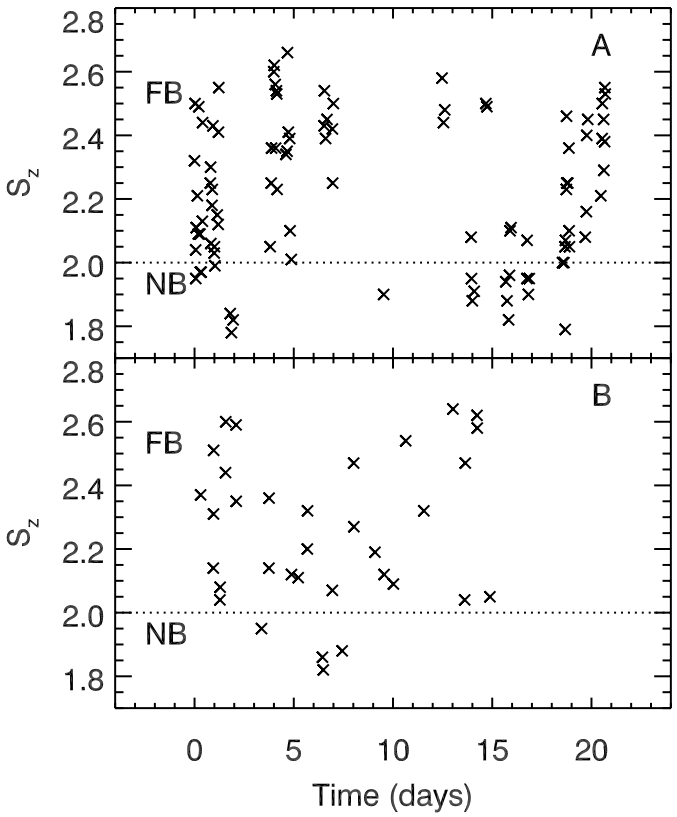

Fig. 3. Variation of mean S_z-parameter in the timescale of several days. Starting date and time for the panel A (January data) are 09/01/98 and 03:50:53 UT respectively and those for panel B (September–October data) are 29/09/98 and 07:07:28 UT respectively. The horizontal lines at $S_z = 2$ represent the NB/FB vertex. It is to be noted that each point here does not correspond to same time-duration.

different fractions of the Z-track during individual observations (Table 1). It spends ∼74% (∼163 ks) of total good time in FB and rest of the time (∼58 ks) in NB. The variation of mean S_z-values (Table 2) over a timescale of several days is shown in Fig. 3. The transitions from NB to FB and vice versa are noticed during several individual observations. For example, the source moves smoothly from lower NB to upper FB during the observation 4 and traces 54% of the Z-track in the timescale of ∼1 hr (see Fig. 4). We also note that the motion of the source along the Z-track is not always smooth and the source jumps occasionally from lower-middle part of NB to lower part of FB and vice versa. Sudden jumps from upper FB to the NB/FB vertex and vice versa have also been observed in a few occasions (see Sect. 4 for discussions). The kinematics of motion is measured in terms of the speed of the source along the Z-track. This speed is defined as $V_z(i) = \mid S_z(i+1) - S_z(i-1) \mid /512$ at a given value of $S_z(i)$ and from several such values, the average speed is calculated for each observation. We find that the source moves with a slower average speed in NB compared to that in FB.

We find two kinds of noise in the power spectra: (1) very-low-frequency-noise (VLFN) and (2) peaked noise (PN). In Table 2, we list the variation of their properties with S_z. It can be seen that in some cases, same (or, nearly same) value of S_z appears more than once in this table. This is because we have not averaged the power spectra over disconnected time intervals. It is also to be noted that due to unavailability of sufficient number of points in upper FB, we have calculated power spectra for S_z-values upto 2.66 (a typical power spectrum consisting of VLFN and PN is shown in Fig. 5). We notice that PN is present (see Table 2) throughout NB and in 70% (previously, it was observed upto 40% (O'Neill et al. 2001)) of the length of FB (from NB/FB vertex). This covers about 75% of the whole Z-track (by "whole Z-track" we mean the Z-track we have obtained in Fig. 1). However, for $S_z \geq 2.47$, the detection of PN is not very significant in most of the cases (see Table 2).

Figure 6 shows the VLFN-index and the properties of PN as the functions of S_z. The VLFN-index does not show any S_z-dependence and its mean value is 1.67 ± 0.07 for the whole Z-track. PN-*FWHM* also does not show any clear evidence of S_z-dependence. However, the average value of the centroid frequency of PN is higher in NB ($\nu_c = 8.1 \pm 0.2$ Hz) than in FB ($\nu_c = 5.68 \pm 0.09$ Hz). The PN-rms-strength does not show any abrupt change at NB/FB vertex, and increases (with almost same rate) from upper NB to the 15% way up the FB (through the NB/FB vertex) and then it decreases. Note that, there is a weak indication of narrow QPO-like features (quality factor $Q > 2$) at $S_z = 2.00 \pm 0.005$ and 2.58 ± 0.06 (during obs. no. 50 and 86^b respectively, see Table 2).

We find that the average value of VLFN-rms-strength, during the January 1998 observations, slowly increases from ∼1% to ∼1.7% with the movement of the source along FB from NB/FB vertex (in NB, it does not show any S_z-dependence; see Fig. 7). However, it shows a different behavior during September–October 1998 observations, as it is stronger in NB than in FB (but note that we have only four S_z points in NB (Fig. 7)).

We investigate the photon energy dependence of PN-rms-strength in FB as well as in NB. We select two S_z ranges from each of these two branches and construct power spectra in the energy bands 2–5.1, 5.1–7, 7–10 and 10–16 keV ranges and

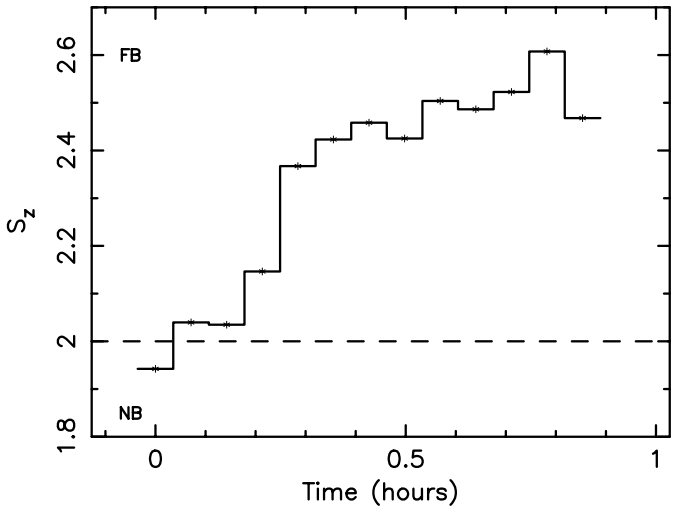

Fig. 4. Variation of mean S_z-parameter with time for the observation 4 (see Table 1). Starting date and time for this plot are 09/01/98 and 08:38:24 UT. Each point has a bin size 256 s. The horizontal line at $S_z = 2$ represents the NB/FB vertex.

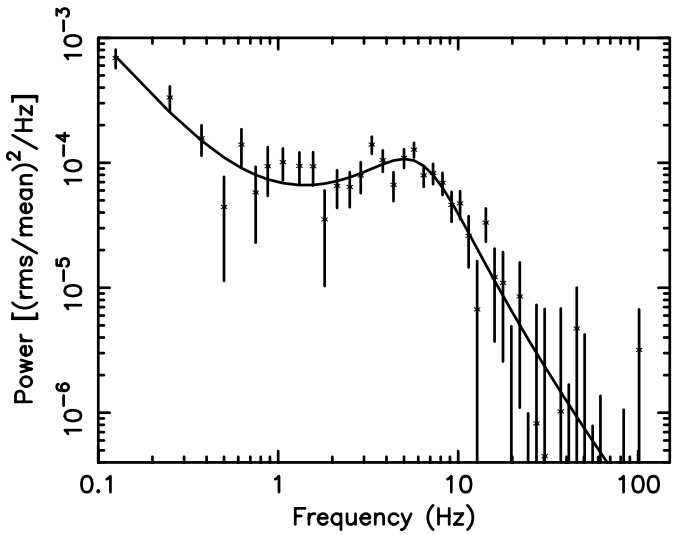

Fig. 5. Power spectrum in the energy band 5.1–60 keV for S_z = 2.31 ± 0.05. The solid line shows the best-fitted curve (power-law+Lorentzian).

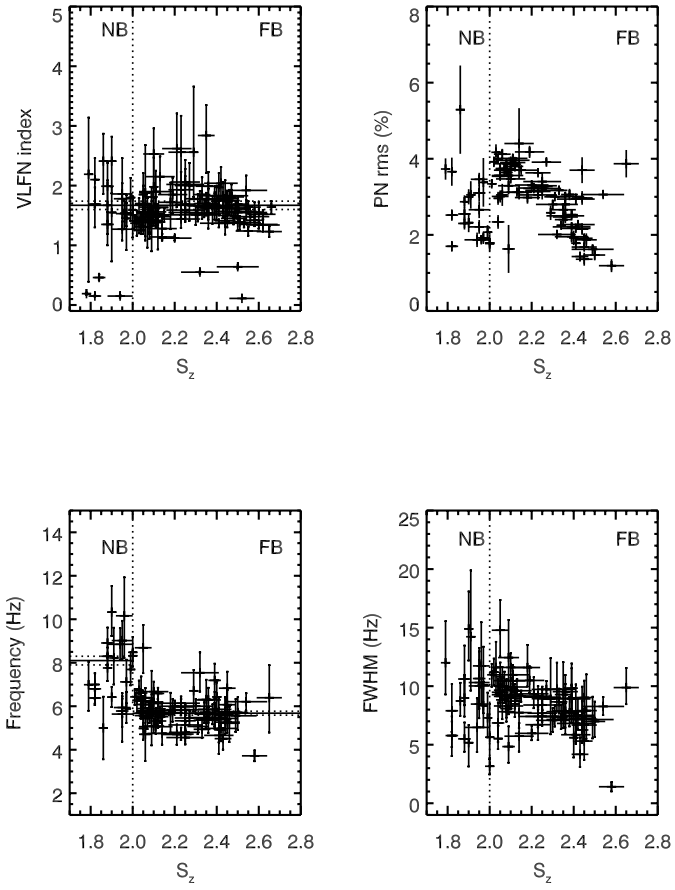

Fig. 6. Properties of VLFN (index) and PN (rms-strength, centroid frequency and *FWHM*) as functions of S_z. Vertical line at $S_z = 2$ in each panel represents the NB/FB vertex. A solid horizontal line in a S_z-region gives the average value of the dependent (i.e., function of S_z) parameter in that region, and the two adjacent (one above and one below) dotted lines correspond to the 1-σ error.

Table 3. The photon energy dependence of rms-strength of PN for four different S_z-values (two from NB and two from FB).

Energy	%rms			
(keV)	$S_z = 1.95 \pm 0.05$	$S_z = 1.86 \pm 0.02$	$S_z = 2.19 \pm 0.07$	$S_z = 2.20 \pm 0.08$
2–5.1	1.78 ± 0.11	1.89 ± 0.21	2.29 ± 0.12	1.84 ± 0.22
5.1–7	2.47 ± 0.21	3.57 ± 0.34	3.60 ± 0.15	3.31 ± 0.27
7–10	3.11 ± 0.26	4.32 ± 0.38	4.13 ± 0.17	4.21 ± 0.25
10–16	2.42 ± 0.73	3.75 ± 0.6	5.01 ± 0.24	2.98 ± 0.95

while fitting the power spectra, ν_c and *FWHM* of PN are fixed at the best-fit values for the broad energy range 5.1–60 keV. We find that the rms-strength of PN shows a positive correlation with the photon energy (upto 10 keV), in both NB and FB (Table 3).

Finally, we compare the CDs of Cyg X-2 at low-overall and high/medium-overall intensity states with that of GX 349+2. We make use of Fig. 1 of Kuulkers et al. (1999) to calculate CDs for Cyg X-2. Both GX 349+2 and Cyg X-2 (at low-overall intensity) show only NB and FB. It is noticed that the transition of Cyg X-2 from high/medium-overall intensity state to low-overall intensity state causes NB/FB vertex to move towards a higher hard color value (Fig. 8).

4. Discussion and conclusions

In this paper, we have carried out the most detailed study to date of the PN properties of the LMXB source GX 349+2 using 31 days (total good-time duration is ~221 ks) of RXTE-PCA data. Unlike most of the earlier observations of GX349+2, the data show a rare, extended normal branch. Therefore, for the first time, it has been possible to compare the properties of NB and FB and address the importance of NB/FB vertex.

In our work, color-color diagram (CD) and hardness-intensity diagram (HID) have been computed with 256 s time average. Such a big time average has been taken in order to

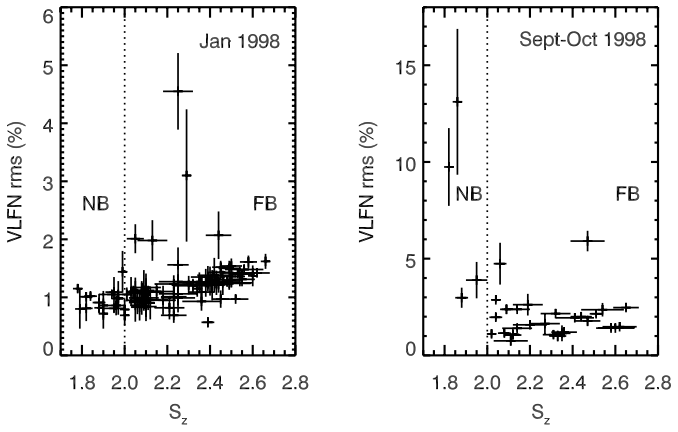

Fig. 7. VLFN-rms-strengths (separately for January 1998 and September–Octobar 1998 data-sets) as functions of S_z. Note that the ranges of vertical axis are different for two panels. Vertical line at $S_z = 2$ in each panel represents the NB/FB vertex.

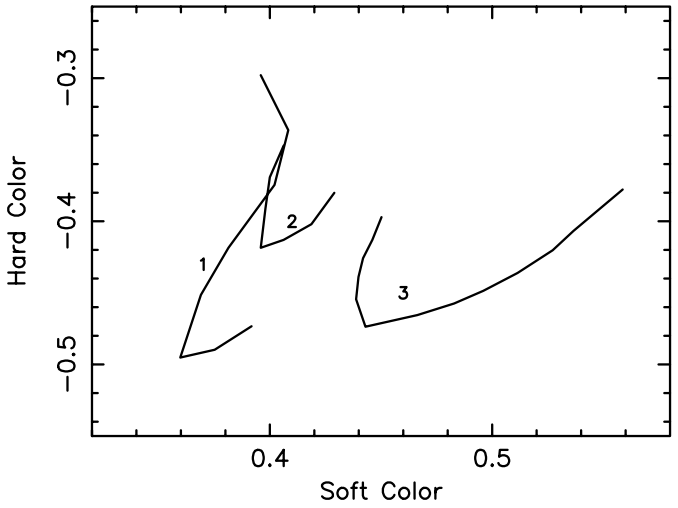

Fig. 8. Comparison between the spectral behaviors of Cyg X-2 (in low-overall intensity state) and GX 349+2. The curve with label "1" is the Z-track for Cyg X-2 in high/medium-overall intensity state and that with label "2" is for low-overall intensity state. These tracks have been generated using Fig. 1 of Kuulkers et al. (1999). The curve with label "3" is the Z-track for GX 349+2. Here the definitions of soft color and hard color are slightly different, i.e., they are the logarithms of soft color and hard color (respectively) used in Fig. 1.

differentiate between the normal branch (NB) and the flaring branch (FB) in an unambiguous way, and even with it, we get sufficient number of points in CD and HID, as we have a fairly large data-set. From the CD and HID, it can be noted that the overall intensity and the broad spectral behavior of the source remain the same for the two sets (January and September–October) of data.

Our analysis shows that for ~74% of the total observation time, the source remained in FB (see Fig. 3 and Table 1). This is in accordance with the fact that GX 349+2 was almost always found to be in FB. We also see (from Table 1) that the source can move in both the directions along the Z-track. One of our interesting findings is that the source can move from upper FB to lower FB or from FB to NB (and vice versa) in the timescale of 256 s (our bin-size in CD and HID). Therefore, any model that tries to explain the movement of the source along the Z-track, must take this timescale (~5 min) into account.

A broad QPO (that is to some extent similar to N/FBO of other Z sources) was reported to be found in the FB of GX 349+2 during all previous observations. By the definition of QPO (quality factor $Q > 2$), this feature in the power spectrum may not be called a QPO. O'Neill et al. (2001) called it "FBN", as they found it mostly in the flaring branch (they had only one S_z-point in NB). However we call it "PN" (following the earlier convention as in Kuulkers & van der Klis 1998), as our analysis shows it in both NB and FB. This is the first quantitative study of the properties of PN in both NB and FB. O'Neill et al. (2001) attempted it with GINGA data, but they did not get an extended normal branch. Our systematic investigation of PN properties with good quality RXTE data reveals that the average value of PN-centroid frequency is slightly higher in NB than in FB. However, PN-*FWHM* and PN-rms-strength do not show any abrupt changes at NB/FB vertex. The energy dependences (upto 10 keV) of PN-rms-strength are also similar in NB and FB. These indicate that PN may not be strongly correlated with the bending of Z-track at NB/FB vertex and the origin of PN in NB and FB is probably same (i.e., should be explained by same theoretical model). This is supported by the fact that PN is not a property of predominantly one of the branches (observed throughout NB and in most of the length of FB).

It is worth comparing the properties of NBO and FBO (together N/FBO) seen in other Z-sources (specially in two Sco-like sources: GX 17+2 and Sco X-1) with those of PN. Based on a few common properties it can be argued that these two phenomena may have similar origin. For example, ν_c for NBO has the value (5–7 Hz) similar to that for PN, and both N/FBO and PN can be fitted by Lorentzian. Besides, the rms-strength of each of N/FBO (Sco X-1; Dieters & van der Klis 2000) and PN (GX 349+2; see Table 3) increases with increasing photon energy (upto 10 keV). In addition, there is no time-lags between high-energy and low-energy photons for both N/FBO and PN (Kuulkers & van der Klis 1998). However, there are several important differences. As mentioned earlier, N/FBO is narrow ($Q > 2$) while PN is broad ($Q < 1$). In addition, while moving from NB to FB, at NB/FB vertex the centroid frequency of N/FBO jumps to a higher (about double) value and then increases continuously along FB. But PN-centroid-frequency decreases slightly at the vertex and then remains almost the same as the source moves along FB. Besides, while PN-*FWHM* does not show any clear dependence on the position along the Z-track, the *FWHM* of N/FBO increases at the NB/FB vertex and continues to increase along FB. The fraction of the track length over which N/FBO and PN appear are also different. For example, for GX 17+2, NBO appears upto 35% of the length of NB from the NB/FB vertex and FBO appears upto 20% of the length of FB from the same vertex (Homan et al. 2002), and these numbers are 50% and 10% respectively (Dieters & van der Klis 2000) for Sco X-1. But for GX 349+2, we see that PN is present in the whole length of NB and in 70% of the length of FB.

The discussion of the previous paragraph clearly shows that a single model for both N/FBO and PN is very difficult to formulate. According to the standard model for N/FBO (Fortner et al. 1989; Lamb 1991; Psaltis et al. 1995), radial oscillations in the optical depth of radial inflow (caused by the radiation pressure at near-Eddington-luminosity) produce a rocking in the X–ray spectrum which gives rise to NBO. Although this model may be able to explain N/FBO of Sco X-1, it can not explain PN, as PN-frequency does not increase with the 'inferred accretion rate' in FB. Besides for our case, PN has been observed 70% of the way up the FB. According to the standard model, oscillations are supposed to be suppressed at such a high accretion rate. An alternative model (Titarchuk et al. 2001), that identifies NBO-frequency as the spherical-shell-viscous-frequency, is also not adequate to explain PN.

A peaked noise was observed for the Cyg-like Z source Cyg X-2 (Kuulkers et al. 1999) at low-overall intensities. The noise-component extends from 2 Hz to 20 Hz in the power spectrum, peaking near 6–7 Hz (%rms = 3). These values of centroid frequency and rms-strength are similar to those of PN for GX 349+2. To investigate whether the peaked noise components of GX 349+2 and Cyg X-2 have the same origin, we have computed the CD of GX 349+2 using the same energy ranges as given in Kuulkers et al. (1999). We find (Fig. 8) that at low-overall intensities, the Z-track of Cyg X-2 looks similar (except for a difference in soft color values) to that of GX 349+2 (neither of them shows HB). The hard-color value of the NB/FB vertex for Cyg X-2 increases (i.e., shifts towards that for GX 349+2), when its overall intensity changes from high/medium to low state. This suggests that the nature of the X–ray emitting components of GX 349+2 and that of Cyg X-2 (at low-overall intensities) may be similar to some extent and the intensity in the energy range 6.4–16.0 keV (used to calculate hard color) is an important parameter for more detailed studies. If the origin of peaked noise components of the two sources is similar, then such noise components may be originated in the region, which produces most of the 6.4–16.0 keV luminosity. This is supported by the fact that the rms-strength of PN is higher in this energy range than at lower energies (see Table 3). However, as the CD represents a rough spectral behavior, to establish a connection between the two PN components, it is essential to compare the energy spectra of these two sources in detail.

It is to be noted that Zhang et al. (1998) discovered two kHz QPOs (centroid frequency ~712 Hz and 978 Hz) analyzing the January 1998 data. However the September–October 1998 data do not show any kHz QPO.

Subsequent to our analysis, O'Neill et al. (2002) have submitted a paper analyzing the January 1998 RXTE-PCA data (this is a part of the data-set we have analyzed) for GX 349+2. We note that our results broadly tally with theirs. The primary objective of our work has been to study the properties of PN with S_z-values in detail. However, O'Neill et al. (2002) stressed on the study of VLFN and tried to detect power spectral features (like HBO and sub-HBO) seen in other Z sources.

As mentioned in Sect. 1, GX 349+2 is not a well-observed source and certainly is the most poorly understood one among the Z sources. However, it shows interesting phenomena like PN (which is probably also observed from Cyg X-2 for a particular position of Z-track in CD). Therefore, the study of this source may be very important to understand the physics behind the tracks traced by the Z sources in CD and HID. The detailed study of GX 349+2 in this paper will be useful for this purpose, as well as will help one to formulate a correct theoretical model for PN.

Acknowledgements. We deeply acknowledge P. Sreekumar for providing all the facilities and for detailed discussions. We thank A.R. Rao for reading the manuscript and giving valuable suggestions. We also thank Dipankar Bhattacharya for his help and the Director of the Raman Research Institute for the facilities provided. We are grateful to the referee E. Morgan for his constructive comments and suggestions.

References

Dieters, S. W., & van der Klis, M. 2000, MNRAS, 311, 201
Fortner, B., Lamb, F. K., & Miller, G. S. 1989, Nature, 342, 775
Hasinger, G., & van der Klis, M. 1989, A&A, 225, 79
Hasinger, G., van der Klis, M., Ebisawa, K., Dotani, T., & Mitsuda, K. 1990, A&A, 235, 131
Hertz, P., Vaughan, B., Wood, K. S., et al. 1992, ApJ, 396, 201
Homan, J., van der Klis, M., Jonker, P. G., et al. 2002, ApJ, 568, 878
Kuulkers, E., Homan, J., van der Klis, M., Lewin, W. H. G., & Mendez, M. 2002, A&A, 382, 947
Kuulkers, E., & van der Klis, M. 1996, A&A, 314, 567
Kuulkers, E., & van der Klis, M. 1998, A&A, 332, 845
Kuulkers, E., van der Klis, M., Oosterbroek, T., et al. 1994, A&A, 289, 795
Kuulkers, E., van der Klis, M, Oosterbroek, T., van Paradijs, J., & Lewin, W. H. G. 1997, MNRAS, 287, 495
Kuulkers, E., van der Klis, M., & Vaughan, B. A. 1996, A&A, 311, 197
Kuulkers, E., Wijnands, R., & van der Klis, M. 1999, MNRAS, 308, 485
Lamb, F. K. 1991, Unified Model of X–ray Spectra and QPOs in Low Mass Neutron Star Binaries, ed. J. Ventura, & D. Pines, Neutron Stars: Theory and Observations (Dordrecht, Kluwer Academic Publishers), 445
O'Neill, P. M., Kuulkers, E., Sood, R. K., & Dotani, T. 2001, A&A, 370, 479
O'Neill, P. M., Kuulkers, E., Sood, R. K., & van der Klis, M. 2002 [astro-ph/0204362]
Ponman, T. J., Cooke, B. A., & Stella, L. 1988, MNRAS, 231, 999
Psaltis, D., Lamb, F. K., & Miller, G. S. 1995, ApJ, 454, L137
Smale, A. P. 1998, ApJ, 498, L141.
Titarchuk, L. G., Bradshaw, C. F., Geldzahler, B. J., & Fomalont, E. B. 2001, ApJ, 535, 45
van der Klis, M. 1995, Rapid Aperiodic Variability in X-ray binaries, ed. W. H. G. Lewin, J. van Paradijs, & E. P. J. van den Heuvel, X-ray binaries (Cambridge University Press, Cambridge), 252
van der Klis, M. 2000, ARA&A, 38, 717
Zhang, W., Strohmayer, T. E., & Swank, J. H. 1998, ApJ, 500, 167